MARSHALL GRANT

IN-34-CR

99101

36 P.

CLOSURE MODELS OF TURBULENT THIRD-ORDER MOMENTUM AND TEMPERATURE FLUCTUATIONS

October 1987

R. S. Amano - Principal Investigator
and
J. C. Chai - Research Assistant

Department of Mechanical Engineering
University of Wisconsin--Milwaukee

Status Report

The report documents research completed during the period of May 1987 through September 1987 under NASA-Marshall Space Flight Center Research Grant No. NAG 8-617.

TECHNICAL REPORT STANDARD TITLE PAGE

1. REPORT NO.	2. GOVERNMENT ACCESSION NO.	3. RECIPIENT'S CATALOG NO.

4. TITLE AND SUBTITLE	5. REPORT DATE
Closure Models of Turbulent Third-Order Momentum and Temperature Fluctuations	October 1987
	6. PERFORMING ORGANIZATION CODE
7. AUTHOR(S)	8. PERFORMING ORGANIZATION REPORT #
R. S. Amano and J.C. Chai	
9. PERFORMING ORGANIZATION NAME AND ADDRESS	10. WORK UNIT NO.
University of Wisconsin Milwaukee, WI 53201	
	11. CONTRACT OR GRANT NO. NAG 8-617
	13. TYPE OF REPORT & PERIOD COVERED Status Report May 1987 - September 1987
12. SPONSORING AGENCY NAME AND ADDRESS NASA Washington, DC 20546	14. SPONSORING AGENCY CODE

15. SUPPLEMENTARY NOTES

Point of Contact: Technical Monitor, Dr. Charles Schafer
NASA Marshall Space Flight Center, ALABAMA 34812

16. ABSTRACT

A study is made for the development and computations of the separating and reattacing shear flows. The highlight of the study is an attempt to predict the third-moments of turbulent velocity which is responsible for the diffusion transport of the Reynolds stresses. The present computations show that the third-moments obtained by employing the low-Reynolds number model of transport equations improve the prediction of the third-moments.

The modeling for scalar variables are also performed for the heat transfer computations. Since the transport equations for $\langle u_j\theta \rangle$ and $\langle u_iu_j\theta \rangle$ have been given in the last NASA CR, the study has been extended further to the modeling of $\langle \theta^2 \rangle$, $\langle u_j\theta^2 \rangle$ and ε_θ (dissipation rate for $\langle \theta^2 \rangle$). The formulations are shown in this report.

17. KEY WORDS	18. DISTRIBUTION STATEMENT
Turbulence Models Third-Order Closure Turbulent Heat Transfer	Unclassified - Unlimited

19. SECURITY CLASSIF. (of this report)	20. SECURITY CLASSIF. (of this page)	21. NO. OF PAGES	22. PRICE
Unclassified	Unclassified		

TABLE OF CONTENTS

SUMMARY

A study is made for the development and computations of the separating and reattacing shear flows. The highlight of the study is an attempt to predict the third-moments of turbulent velocity which is responsible for the diffusion transport of the Reynolds stresses. The present computations show that the third-moments obtained by employing the low-Reynolds number model of transport equations improve the prediction of the third-moments.

The modeling for scalar variables are also performed for the heat transfer computations. Since the transport equations for $\langle u_i\theta \rangle$ and $\langle u_i u_j \theta \rangle$ have been given in the last NASA CR, the study has been extended further to the modeling of $\langle \theta^2 \rangle$, $\langle u_i \theta^2 \rangle$ and ε_θ (dissipation rate for $\langle \theta^2 \rangle$). The formulations are shown in this report.

INTRODUCTION

Separation and recirculation of flow is encountered in a vast array of engineering applications. This phenomenon of flow separation and recirculation associates itself with higher turbulence levels which not only render the flow greater analytical complexity but also would result in highly augmenting its heat transfer and momentum aspects. Thus, demand for mathematical models that can predict any complex turbulent flows is increasing as well as experimental measurements for better understanding of such complex flows. It has been observed by many researchers [1,2] that non-isotropic turbulence effects are quite significant in separating shear flows and consequently occurring reattaching and recirculating flows beyond a step. Moreover, turbulent third-moments and corresponding triple scalar-velocity products are equally predominant in the separated shear flow field interacting with turbulent boundary layers.

The most noticeable features of the experimental observations reported by Chandrsuda and Bradshaw [1] and later by Driver and Seegmiller [3] are that the shapes of the third-order moments of turbulence fluctuating velocity change rapidly along the separated shear layer due to distortion of the large eddies by effectively irrotational mechanisms. The implication of these observations in separating and reattaching shear layer is that algebraic relations between the third-order moments and the Reynolds stresses are likely to be inadequate for strongly perturbed flows, making it necessary to use transport equations for the third-moments.

This study is conducted to develop new models of turbulence with the third-order closure in order to predict the turbulent flow through a duct with a relatively complex geometry. As a basic study of modeling, a backward-facing step is chosen to carry out computations. The advantage of having such a flow

geometry is that a number of experimental data are available in the literature for comparison with present results. Computations of the momentum and temperature fields in the flow domain being considered entail the solution of the time-averaged transport equations containing the second-order turbulent fluctuating products. The third-order products, which are responsible for the diffusive transport of the second-order products, attain greater significance in separating and reattaching flows. The following chapter describes the modeling of these transport equations.

MATHEMATICAL MODELS FOR THIRD-MOMENTS

The transport equations for the Reynolds stresses can be given as

$$\frac{\partial}{\partial x_k}\left(U_k \langle u_i u_j \rangle\right) = P_{ij} - \epsilon_{ij} + \phi_{ij} + D_{ij} \tag{1}$$

where P_{ij} and ϕ_{ij}, respectively, represent the production and the pressure-strain rates. In the parenthesis of the above equations, the upper case letter U and the lower case letter u represent the Reynolds averaged and the instantaneous values of the velocity, respectively. The symbol < > denotes that the argument inside this bracket is ensemble-averaged. The pressure-strain correlation ϕ_{ij} is evaluated by using the model of Launder et al. [4].

The diffusion rate, D_{ij}, contains the terms given as follows:

$$D_{ij} = -\frac{\partial}{\partial x_k}\left[\langle u_i u_j u_k \rangle + \frac{\langle u_i p \rangle}{\rho}\delta_{jk} + \frac{\langle u_j p \rangle}{\rho}\delta_{ik}\right.$$

$$\left. - \nu\left(\frac{\partial \langle u_i u_j \rangle}{\partial x_k} + \left\langle u_j \frac{\partial u_k}{\partial x_i}\right\rangle + \left\langle u_i \frac{\partial u_k}{\partial x_j}\right\rangle\right)\right] \tag{2}$$

where p, ρ, and ν represent, respectively, the turbulent fluctuating pressure, the fluid density and the fluid kinematic viscosity. The symbol δ denotes the Kronecker delta. Since the diffusion rate of the Reynolds stresses is governed by the gradient of the third-moments $\langle u_i u_j u_k \rangle$, it becomes necessary to evaluate the third-moments exactly. Thus, the transport equations for such third-moments are developed and shown as follows.

The third moments, $\langle u_i u_j u_k \rangle$, can be evaluated by formulating their transport equations as

$$\frac{\partial}{\partial x_\ell}\left(U_\ell \langle u_i u_j u_k \rangle\right) = -\Big(\langle u_i u_j u_\ell \rangle \frac{\partial U_k}{\partial x_\ell} + \langle u_j u_k u_\ell \rangle \frac{\partial U_i}{\partial x_\ell} + \langle u_k u_i u_\ell \rangle \frac{\partial U_j}{\partial x_\ell}\Big)$$

(I)

$$+ \Big(\langle u_i u_j \rangle \frac{\partial \langle u_k u_\ell \rangle}{\partial x_\ell} + \langle u_j u_k \rangle \frac{\partial \langle u_i u_\ell \rangle}{\partial x_\ell} + \langle u_k u_i \rangle \frac{\partial \langle u_j u_\ell \rangle}{\partial x_\ell}\Big)$$

(II)

$$- \Big(\langle u_i u_j \frac{\partial u_k u_\ell}{\partial x_\ell} \rangle + \langle u_j u_k \frac{\partial u_i u_\ell}{\partial x_\ell} \rangle + \langle u_k u_i \frac{\partial u_j u_\ell}{\partial x_\ell} \rangle\Big) \qquad (3)$$

(III)

$$- \frac{1}{\rho}\Big(\langle u_i u_j \frac{\partial p}{\partial x_k} \rangle + \langle u_j u_k \frac{\partial p}{\partial x_i} \rangle + \langle u_k u_i \frac{\partial p}{\partial x_j} \rangle\Big)$$

(IV)

$$+ \langle u_i u_j \frac{\partial}{\partial x_\ell} [\nu (\frac{\partial u_k}{\partial x_\ell} + \frac{\partial u_\ell}{\partial x_k})] \rangle$$

$$+ \langle u_j u_k \frac{\partial}{\partial x_\ell} [\nu (\frac{\partial u_i}{\partial x_\ell} + \frac{\partial u_\ell}{\partial x_i})] \rangle$$

$$+ \langle u_k u_i \frac{\partial}{\partial x_\ell} [\nu (\frac{\partial u_j}{\partial u_\ell} + \frac{\partial u_\ell}{\partial x_j})] \rangle$$

(V)

In the above equations, terms I and II represent, respectively, the generation rates due to mean strain and the Reynolds stresses. Term III is responsible for the generation rate if the Gaussian approximation is applied; this can be merged into term II. Term IV, which is the pressure-stress correlation, plays a significant role in redistributing the tensor and in diffusing due to fluctuating pressure. Term V can be divided into the molecular diffusion rate and the dissipation rate.

In order to account for the viscous effects that are predominant near the wall, a low-Reynolds number modification needs to be incorporated in the transport equations of the third-moments.

The theory behind this low-Reynolds number model is based upon the fact that the scale of the eddies created in the shear layer changes rapidly as the flow approaches the solid wall by enhancing the turbulence energy dissipation rate. Thus, the model should be devised to control the size of the eddy. This was done by evaluating the correct expression for the dissipation rate, ε, by formulating it in each layer near the wall such as the viscous sublayer, the buffer layer, and the fully turbulent core flow. This controller is incorporated in the pressure-stress term (Term IV in Eq. (3)) in

order to adjust the time of rate change of the third-moments of turbulence velocity as follows:

$\theta_{ijk} \equiv$ Pressure-stress term

$$= C_\gamma \frac{\varepsilon}{k} \langle u_i u_j u_k \rangle \tag{4}$$

and

$\theta_{ijk,w} \equiv$ near-wall correction for pressure-stress term

$$= C_\gamma \frac{1}{k} \langle u_i u_j u_k \rangle \{\max [C_{\gamma w} \frac{k^{3/2}}{C_\ell y}, 2\nu (\frac{\partial k^{1/2}}{\partial y})^2]\} \tag{5}$$

where k and y represent the turbulence energy and the distance from the wall, respectively.

The dissipation rate is given as:

$\varepsilon_{ijk} \equiv$ Dissipation due to viscous effect

$$= C_{\varepsilon\gamma} \varepsilon k^{1/2} \tag{6}$$

and

$D_{ijk} \equiv$ Diffusion due to viscous effect

$$= \frac{\partial}{\partial x_\ell} (\nu \frac{\partial}{\partial x_\ell} \langle u_i u_j u_k \rangle) \tag{7}$$

The values for the constants are listed in Table 1.

TABLE 1. Recommended values for the constants

C_g	C_ℓ	C_γ	$C_{\gamma w}$	$C_{\varepsilon\gamma}$
1.0	2.55	3.0 (low-Re no. model) 5.8 (high-Re no. model)	8.0	0.2

The models considered in this study are defined as follows:

<u>High-Reynolds number model</u>

$$\frac{\partial}{\partial x_\ell}\left(U_\ell \langle u_i u_j u_k\rangle\right) = P_{ijk,1} + P_{ijk,2} + \theta_{ijk} + D_{ijk} \tag{8}$$

where

$P_{ijk,1} \equiv$ production due to mean strains

$$= -C_g\left(\langle u_i u_j u_\ell\rangle \frac{\partial U_k}{\partial x_\ell} + \langle u_j u_k u_\ell\rangle \frac{\partial U_i}{\partial x_\ell} + \langle u_k u_i u_\ell\rangle \frac{\partial U_j}{\partial x_\ell}\right) \tag{9}$$

$P_{ijk,2} \equiv$ Production due to Reynolds stresses interacting with their gradients

$$= -\left(\langle u_k u_\ell\rangle \frac{\partial \langle u_i u_j\rangle}{\partial x_\ell} + \langle u_i u_\ell\rangle \frac{\partial \langle u_j u_k\rangle}{\partial x_\ell} + \langle u_j u_\ell\rangle \frac{\partial \langle u_k u_i\rangle}{\partial x_\ell}\right) \tag{10}$$

<u>Low-Reynolds number model</u>

$$\frac{\partial}{\partial x_\ell}\left(U_\ell \langle u_i u_j u_k\rangle\right) = P_{ijk,1} + P_{ijk,2} + \theta_{ijk} + \theta_{ijk,w} + \varepsilon_{ijk} + D_{ijk} \tag{11}$$

SOLUTION PROCEDURE

Figure 1 shows the solution domain of the flow field. The inlet section is located approximately two step heights upstream from the step and the outlet section about sixty step heights downstream therefrom. After several grid tests it was discerned that the system with 62 x 62 node points gives results independent of the grid. More details are given in the following chapter. The computations were performed using the 62 x 62 variable grid with the grid expanding linearly at the rate of 2% in x-direction and at 3% in y-direction. Figure 2 shows the numerical grid used in computations (5:1 expansion in y-direction).

Computations of the transport equations described in the preceding section are achieved by using the finite volume method [5]. The iterative procedure is terminated when the maximum value of the relative residual sources of U, V, and mass balance falls below 1%. However, the computations of the triple products are continued until the relative residual sources fall below 3×10^{-8}.

RESULTS AND DISCUSSION

Figures 3 and 4 show the computed skin friction coefficient, C_f, and pressure coefficient, C_p, respectively, along the bottom wall. The results are also compared with the experimental data of Driver and Seegmiller [3]. These coefficients are defined as follows:

$$C_f = \frac{\tau_w}{\frac{1}{2} \rho U_{IN}^2} \tag{12}$$

$$C_p = \frac{P - P_{ref}}{\frac{1}{2} \rho U_{IN}^2} \tag{13}$$

where τ_w and P represent the wall shear stress and the Reynolds averaged pressure, respectively. The subscript IN stands for inlet and ref indicates the reference location which is two step heights upstream of the step.

Computations have been performed with several different grid systems ranging from 32 x 32 to 62 x 62. It is shown in these figures that fair grid independent status is attained with the grid system finer than 52 x 52. For this reason the grid with 62 x 62 has been used in the rest of the computations. The agreement between the computation and the measured data is reasonably well except the discrepancy for the pressure coefficient beyond the reattachment point.

Figure 5 shows the mean velocity profiles at two downstream locations. The computed profiles are compared with the experimental data taken by Chandrsuda and Bradshaw [1]. The measured data were obtained by using two different methods: one by pressure-probe and the other by hot-wire. Agreement between the computation and the two sets of the experiment is quite reasonable. It is also noticed that the trend of the computed results accords more with the hot-wire measurements than with the pressure-probe data.

Figure 6 shows the profiles of the Reynolds stresses at several locations downstream of the step. As seen in this figure agreement of the normal stresses (<uu> and <vv>) and the shear stress (<uv>) between computed results and the measurement is fairly well within the error of 10% beyond the reattachment position; however, the computed <uu> and <uv> profiles within the recirculating region do not agree with the measured levels at the peak positions. This disagreement seems to be larger near the step, but both results coincide toward far downstream.

Probably, the generation rate and the pressure-strain correlation associated with the secondary mean strain rates ($\partial V/\partial x$) for the transport

equation of <uv> is not as high as it should be in this near step region, whereas the actual shear stress level might be enhanced due to the cornering flow at the bottom of the step.

Figure 7 represents the comparison of the third-moments of turbulence fluctuating velocity between the high-Reynolds number and low-Reynolds number models. In this figure large changes are observed between these two models. The high-Reynolds number model gives higher levels in the near-wall region than the low-Reynolds number model. This fact indicates that the terms represented by Eqs. (5) and (6) play a significant role in the determination of the third-moments. In the near-wall region, the eddies created through the separated shear layer tend to become smaller, and as a result, the rate of turbulence energy dissipation increases rapidly. This is why the effect of ε added in the model promotes the dissipation action of $\langle u_i u_j u_k \rangle$ in the near-wall region giving lower levels of the third-moments toward the solid wall. Agreement of the computations by the low-Reynolds number model, thus, is considerably improved.

Figure 8 represents the comparisons of the low-Reynolds number model with other algebraic models developed by several researchers: Hanjalic and Launder [6], Cormack et al. [7], Daly and Harlow [8], and Shir [9]. As shown in this figure, the results obtained by the transport equations for the third-moments give generally better agreement with the experimental data than the results obtained by using the corresponding algebraic models. However, it is also noticed that the levels of the third-moments predicted by using the transport equations are very high across the separated shear layer above the recirculating flow, although they agree reasonably well with the experimental data at the location near the reattachment and the downstream region.

Another advantage of using the transport equations is that a low-Reynolds number correlation can be incorporated in order to account for the viscous effect near the wall as well as the convection effect. Thus, the prediction by using the transport equations is closer to the measured data near the wall throughout the flow region.

The above discussion can be summarized as follows:

1. The Reynolds-stress model developed in this study is shown to predict the separating and reattaching shear flows properly.
2. The third-order turbulence velocity fluctuating tensor denotes rapid changes in the reattaching and recirculating flow regions. This behavior can be predicted by developing the transport equations for the third-moments of turbulence velocity.
3. It was shown that by promoting the dissipation effect of the third-moments in the near-wall region the prediction of the third-moments were considerably improved. This low-Reynolds number model for the third-moments provides more universal results than do the algebraic models.

Figures 9-11 show variations of the computed Reynolds stresses. Figures 12-15 show variations of the triple products of the velocity fluctuations. It is clear that the sharp changes in the levels of the triple products are produced in the separating shear flow region which diminish toward downstream.

DEVELOPMENT OF TEMPERATURE FLUCTUATING EQUATIONS

A new model has been under developing for the computation of heat transfer rates in a separating and recirculating flow. Since a transport equation approach is required for better prediction of such complex flows, temperature fluctuating variables with interaction with velocity fluctuating

transport are correlated with defined hydrodynamic and Reynolds averaged velocity fluctuations.

In the last report [10] the formulations and the preliminary computed results were shown for the variables of $\langle u_i\theta\rangle$ and $\langle u_i u_j\theta\rangle$. In this report formulations of other variables such as

$$R_{\theta\theta} = \langle\theta^2\rangle/2 \tag{14}$$

$$R_{i\theta\theta} = \langle u_i\theta^2\rangle \tag{15}$$

and

$$\varepsilon_\theta = \alpha\left\langle\frac{\partial\theta}{\partial x_j}\frac{\partial\theta}{\partial x_j}\right\rangle \tag{16}$$

are presented where α and θ denote, respectively, the thermal diffusivity and fluctuating component of temperature. ε_θ, which represents the dissipation rate of turbulence temperature energy level, corresponds to ε.

The transport equation for $R_{\theta\theta}$ was developed because it appears in the buoyant source term of the vertical heat flux equation of stratified flows. For this reason the transport equations for ε_θ and $R_{i\theta\theta}$ were developed in order to close the $R_{\theta\theta}$ equation. The buoyant term is important because a fluid element receives an upthrust (buoyant effect) proportional to $\alpha\theta g$ if its instantaneous temperature exceeds the average temperature at the horizontal plane by θ. This will produce an extra enthalpy flux proportional to $\alpha\theta g(T + \theta)$ which upon time averaging reduces to $\alpha g R_{\theta\theta}$ and increases the overall levels of $\langle v\theta\rangle$ [11].

Scalar Double Product $R_{\theta\theta}$

Transport equation for $R_{\theta\theta}$ is given as:

$$U_j \frac{\partial R_{\theta\theta}}{\partial x_j} = - \langle u_j \theta \rangle \frac{\partial T}{\partial x_j} - \varepsilon_\theta - \frac{\partial}{\partial x_j} \left[\langle R_{j\theta\theta} \rangle - \alpha \frac{\partial R_{\theta\theta}}{\partial x_j} \right] \qquad (17)$$

(i) (ii) (iii) (iv) (v)

Equation (17) is explained as follows:

(i) Rate of change of turbulence temperature energy level balances with

(ii) Production of turbulence temperatures energy by mean temperature gradient

minus

(iii) Energy dissipation rate of turbulence temperature by molecular action

plus

(iv) Diffusion transport due to turbulence velocity fluctuation

plus

(v) Diffusion transport due to molecular action

The dissipation rate for the double product of the temperature fluctuations, ε_θ, is obtained in a similar manner as is done for ε.

$$U_j \frac{\partial \varepsilon_\theta}{\partial x_j} = - 2 \alpha \left\langle \frac{\partial \theta}{\partial x_j} \frac{\partial u_k}{\partial x_j} \right\rangle \frac{\partial T}{\partial x_k} - 2 \alpha \left\langle u_k \frac{\partial \theta}{\partial x_j} \right\rangle \frac{\partial^2 T}{\partial x_k \partial x_j}$$

(i) (ii) (iii)

$$- 2 \alpha \left\langle \frac{\partial \theta}{\partial x_j} \frac{\partial \theta}{\partial x_k} \right\rangle \frac{\partial U_k}{\partial x_j} - 2 \alpha \left\langle \frac{\partial \theta}{\partial x_j} \frac{\partial u_k}{\partial x_j} \frac{\partial \theta}{\partial x_k} \right\rangle \qquad (18)$$

(iv) (v)

$$- 2 \left\langle \alpha \frac{\partial^2 \theta}{\partial x_j \partial x_k} \right\rangle^2 - \frac{\partial}{\partial x_j} \left[\langle \varepsilon'_\theta u_j \rangle - \alpha \frac{\partial \varepsilon_\theta}{\partial x_j} \right]$$

(vi) (vii) (viii)

where

$$\varepsilon_\theta' = \alpha \frac{\partial \theta}{\partial x_j} \frac{\partial \theta}{\partial x_j}: \quad \text{Unaveraged quantity}$$

Equation (18) is interpreted as follows:

(i) Rate of change of ε_θ

balances with

(ii) Generation due to mean temperature gradient

plus

(iii) Secondary generation due to mean temperature gradient

plus

(iv) Generation due to mean vortex stretching action

plus

(v) Generation due to turbulence fluctuations

minus

(vi) Destruction of ε_θ due to fine scale turbulence interactions

plus

(vii) Diffusion rate due to turbulence velocity

plus

(viii) Diffusion rate due to molecular action.

It is generally recognized that the contribution of terms (ii), (iii) and (iv) is negligibly small in high turbulent flows. Thus these terms can be dropped.

Terms (v) and (vi) are treated in the same manner as ε:

$$(v) + (vi) = [C_{\varepsilon\theta_1} P_\theta - C_{\varepsilon\theta_2} \varepsilon_\theta] \frac{\varepsilon_\theta}{R_{\theta\theta}} \tag{19}$$

where

$$P_\theta = - \langle u_k \theta \rangle \frac{\partial T}{\partial x_k} \tag{20}$$

Term (vii) may be given as

$$- \frac{\partial}{\partial x_j} [\langle \varepsilon_\theta' u_j \rangle] = - \frac{\partial}{\partial x_j} [C_{\varepsilon D} \frac{R_{\theta\theta}}{\varepsilon_\theta} \langle u_j \theta \rangle \frac{\partial \varepsilon_\theta}{\partial x_j}] \tag{21}$$

Thus Eq. (18) becomes

$$U_j \frac{\partial \varepsilon_\theta}{\partial x_j} = \frac{\partial}{\partial x_j} [\alpha \frac{\partial \varepsilon_\theta}{\partial x_j} - C_{\varepsilon D} \frac{R_{\theta\theta}}{\varepsilon_\theta} \langle u_j \theta \rangle \frac{\partial \varepsilon_\theta}{\partial x_j}] + [C_{\varepsilon\theta_1} P_\theta - C_{\varepsilon\theta_2} \varepsilon_\theta] \frac{\varepsilon_\theta}{R_{\theta\theta}} \tag{22}$$

$R_{i\theta\theta}$ in Eq. (17) is still undetermined. This is modeled currently as

$$U_j \frac{\partial R_{i\theta\theta}}{\partial x_j} = \underbrace{- 2 \langle u_i u_j \theta \rangle \frac{\partial T}{\partial x_j}}_{\text{(i)}} \underbrace{- \langle u_j \theta^2 \rangle \frac{\partial U_i}{\partial x_j}}_{\text{(ii)}} \underbrace{- [2 \langle u_j \theta \rangle \frac{\partial \langle u_i \theta \rangle}{\partial x_j} + \langle u_i u_j \rangle \frac{\partial \langle \theta^2 \rangle}{\partial x_j}]}_{\text{(iii)}} \tag{23}$$

$$\underbrace{- \frac{\partial}{\partial x_j} [C_D \frac{R_{\theta\theta}}{\varepsilon_\theta} \langle u_j \theta \rangle \frac{\partial R_{i\theta\theta}}{\partial x_j}]}_{\text{(iv)}} + \underbrace{2 \alpha \langle \frac{\partial}{\partial x_j} (u_i \theta \frac{\partial \theta}{\partial x_j}) \rangle}_{\text{(v)}} + \underbrace{\nu \langle \frac{\partial}{\partial x_j} (\theta^2 \frac{\partial u_i}{\partial x_j}) \rangle}_{\text{(vi)}}$$

$$\underbrace{+ \langle \frac{p}{\rho} \frac{\partial \theta^2}{\partial x_i} \rangle}_{\text{(vii)}} \underbrace{- \langle \theta^2 \frac{\rho'}{\rho} \rangle g \delta_{i2}}_{\text{(viii)}}$$

Equation (23) may be explained as

(i) Rate of change of $\langle u_i \theta^2 \rangle$

is balanced with

(ii) Generation due to mean temperature gradient

plus

(iii) Generation due to mean vortex sketching

plus

(iv) Generation due to turbulence

plus

(v) Diffusion due to turbulence

plus

(vi) Diffusion due to thermal molecular action

plus

(vii) Diffusion due to momentum molecular action

plus

(viii) Pressure-scalar correlation

minus

(ix) Buoyancy effect.

The pressure-scalar correlation is split into two terms as

$$\left\langle \frac{p}{\rho} \frac{\partial \theta^2}{\partial x_i} \right\rangle = C_{p1} \langle u_i \theta^2 \rangle \frac{\epsilon_\theta}{R_{\theta\theta}} - C_{p2} \langle u_k \theta^2 \rangle \frac{\partial U_i}{\partial x_k} \tag{24}$$

The buoyancy term is given as

$$(ix) = - \langle \theta^2 \rangle \, g \, \frac{\Delta T}{\Delta T_o} \, \delta_{i2} \tag{25}$$

Thus, by neglecting molecular diffusion terms we can solve Eq. (23) after determining coefficients appearing in diffusion (term (v)) and pressure-scalar correlation (Eq. (24)).

REFERENCES

1. Chandrsuda, C. and Bradshaw, P., "Turbulence Structure of a Reattaching Mixing Layer," Journal of Fluid Mechanics, Vol. 110, pp. 171-194, 1981.

2. Eaton, J. K. and Johnston, J. P., "A Review of Research on Subsonic Turbulent Flow Reattachment," AIAA Journal, Vol. 19, No. 9, pp. 1093-1100, 1981.

3. Driver, D. M., and Seegmiller, H. L., "Features of a Reattaching Turbulent Shear Layer in Divergent Channel flow," AIAA Journal, Vol. 23, No. 2, pp. 163-171, 1985.

4. Launder, B. E., Reece, G. J. and Rodi, W., "Progress in the Development of a Reynolds Stress Turbulence Closure," Journal of Fluid Mechanics, Vol. 68, pp. 537-566, 1975.

5. Amano, R. S., Goel, P. and Chai, J. C., "Turbulence Energy and Diffusion Transport in a Separating and Reattaching Flow," AIAA Journal, Vol. 24, No. 11, 1987.

6. Hanjalic, K. and Launder, B. E., "A Reynolds Stress Model of Turbulence and Its Application to Thin Shear Flows," Journal of Fluid Mechanics, Vol. 52, pp. 609-638, 1972.

7. Cormack, D. E., Leal, L. G. and Seinfeld, J. H., "An Evaluation of Mean Reynolds Stress Turbulence Models: The Triple Velocity Correlation," Journal of Fluids Engineering, Vol. 100, pp. 47-54, 1978.

8. Daly, B. J. and Harlow, F. H., "Transport Equations in Turbulence," The Physics of Fluids, Vol. 13, No. 11, pp. 2634-2649, 1970.

9. Shir, C. C., "A Preliminary Numerical Study of Atmospheric Turbulent Flows in the Idealized Planetary Boundary Layer," Journal of Atmospheric Science, Vol. 30, pp. 1327-1339, 1973.

10. Amano, R. S., Goel, P. and Chai, J. C., "A Transport Model of the Turbulent Scalar-Velocity," NASA CR, May 1987.

11. Launder, B. E., "Heat and Mass Transport," in Turbulence-Topics on Applied Physics, (edited by P. Bradshaw), Vol. 12, chapter 6, 1976.

FIGURE CAPTIONS

FIGURE 1. Solution domain--Backward-facing step geometry with the separating, recirculating and redeveloping regions.

FIGURE 2. Numerical grid used in computations.

FIGURE 3. Skin friction coefficient along the bottom wall downstream of the step.

FIGURE 4. Pressure coefficient along the bottom wall.

FIGURE 5. U-velocity profiles downstream of the step.

FIGURE 6. Reynolds-stress profiles downstream of the step.

FIGURE 7. Third-moment profiles downstream of the step: Comparison of the low and high-Reynolds number models.

FIGURE 8. Third-moment profiles downstream of the step: Comparison of the low-Reynolds number model with algebraic models.

FIGURE 9. Variation of $\langle u^2 \rangle$

FIGURE 10. Variation of $\langle v^2 \rangle$

FIGURE 11. Variation of $\langle uv \rangle$

FIGURE 12. Variation of $\langle u^3 \rangle$

FIGURE 13. Variation of $\langle u^2 v \rangle$

FIGURE 14. Variation of $\langle uv^2 \rangle$

FIGURE 15. Variation of $\langle v^3 \rangle$

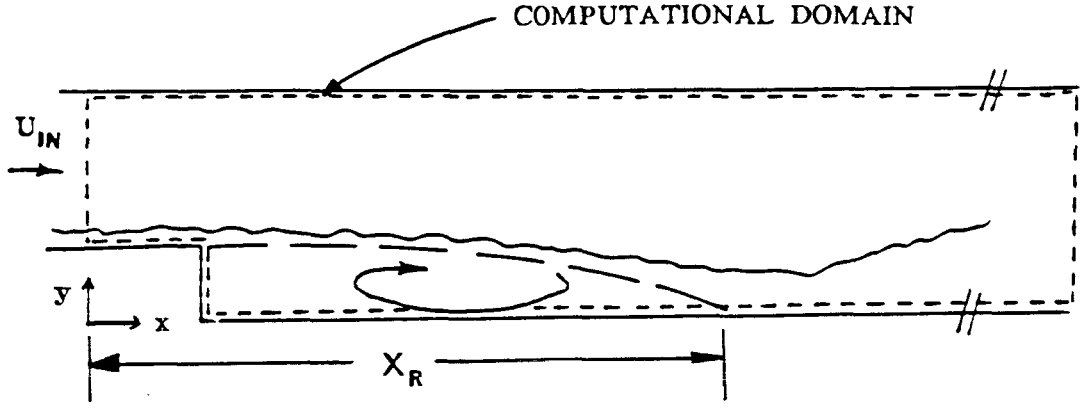

FIGURE 1. Solution domain--Backward-facing step geometry with the separating, recirculating and redeveloping regions.

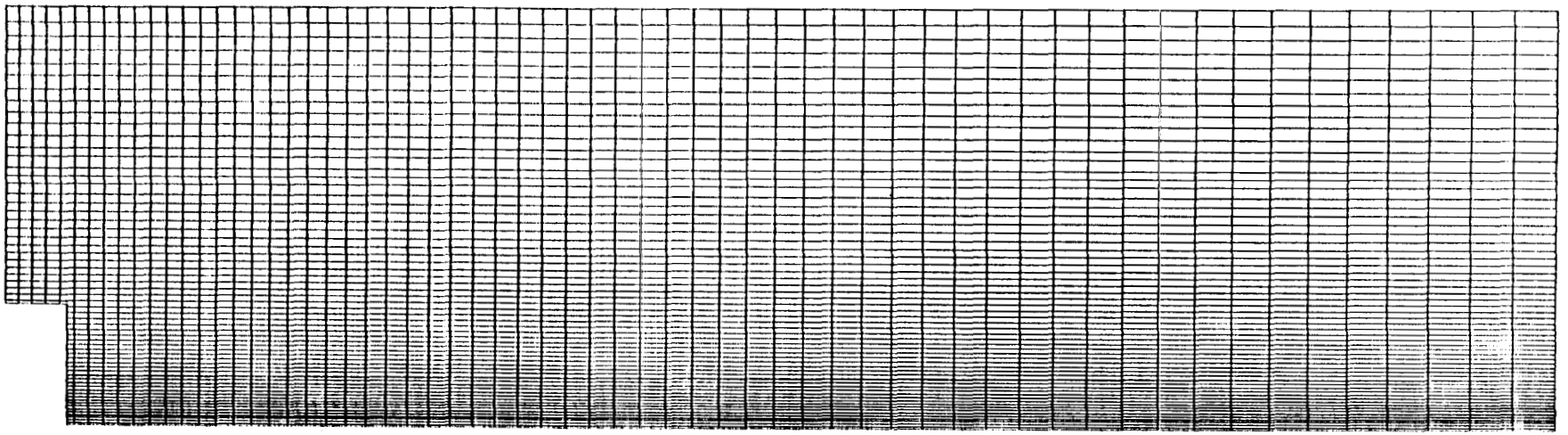

FIGURE 2. Numerical grid used in computations.

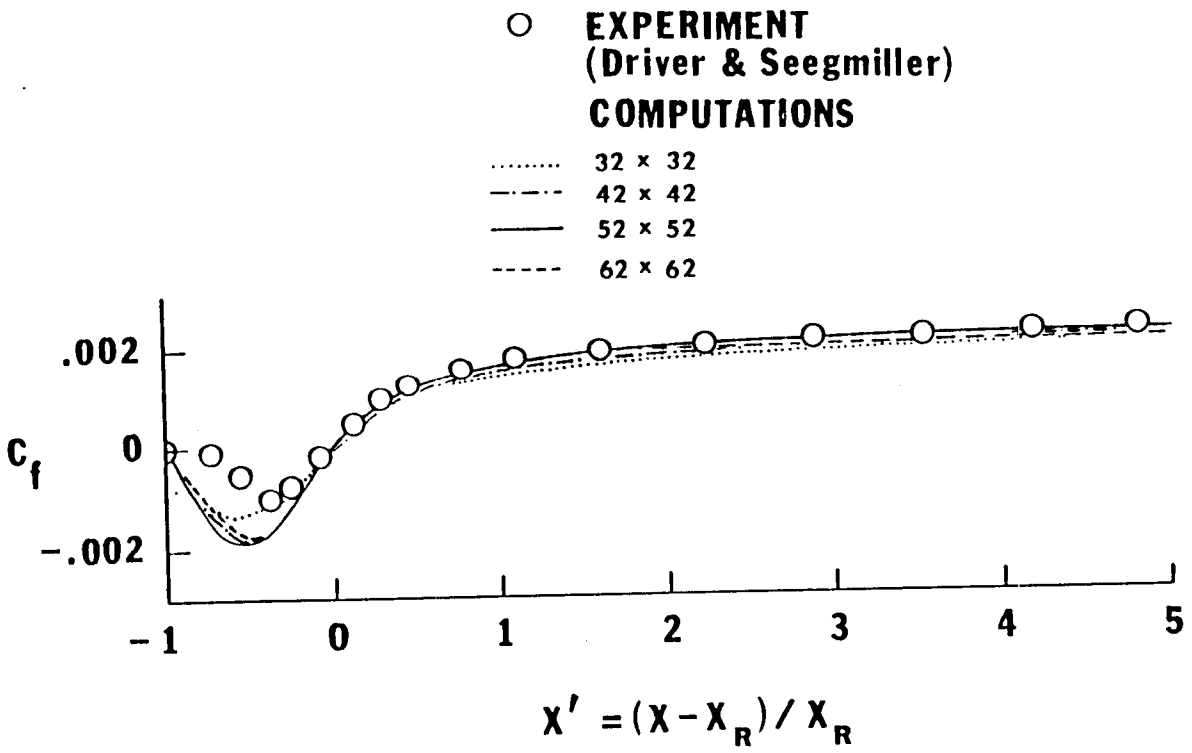

FIGURE 3. Skin friction coefficient along the bottom wall downstream of the step.

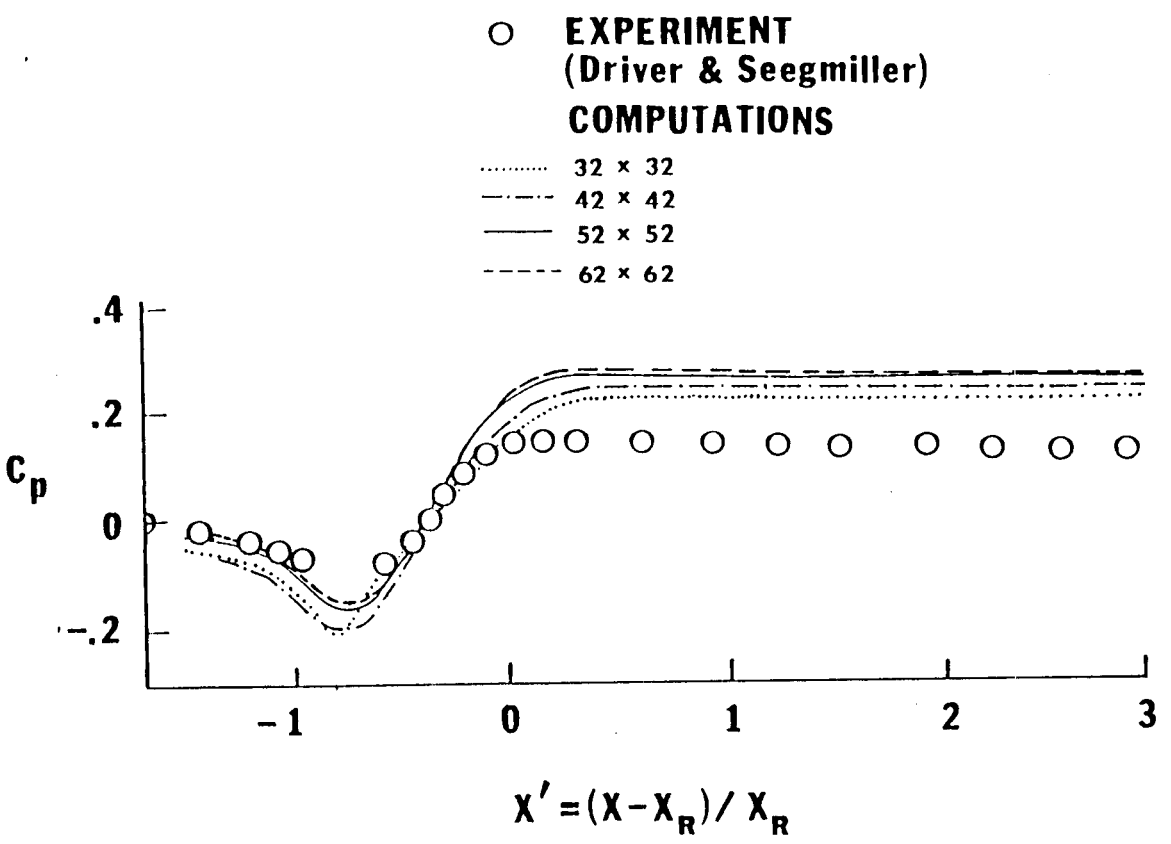

FIGURE 4. Pressure coefficient along the bottom wall.

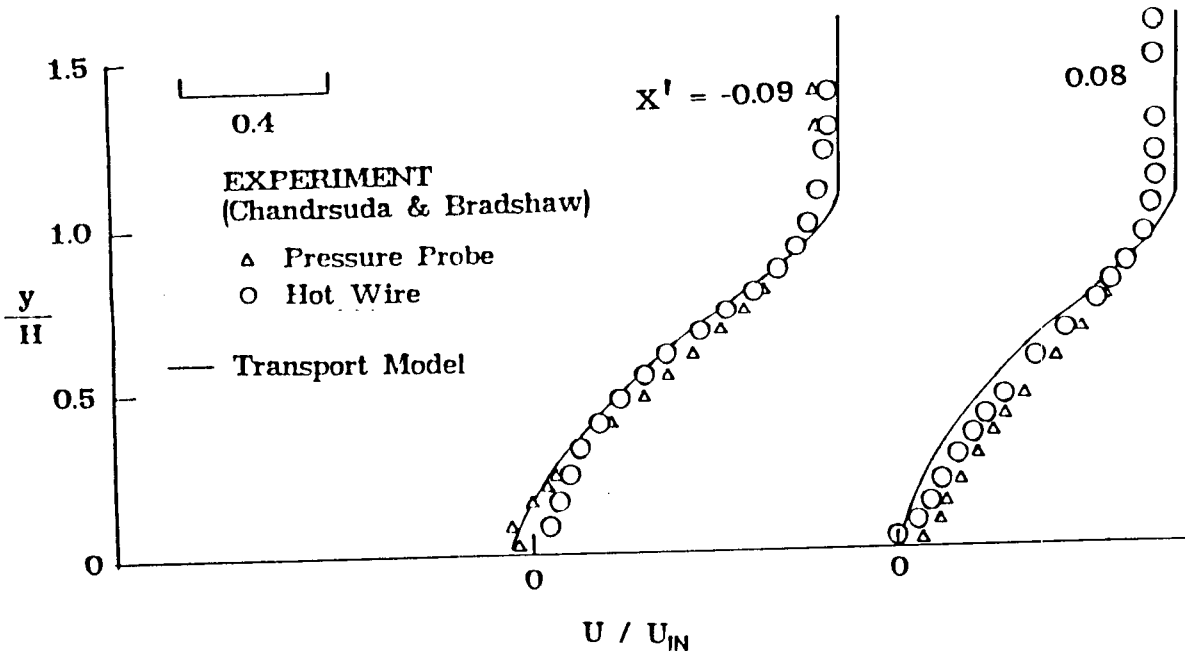

FIGURE 5. U-velocity profiles downstream of the step.

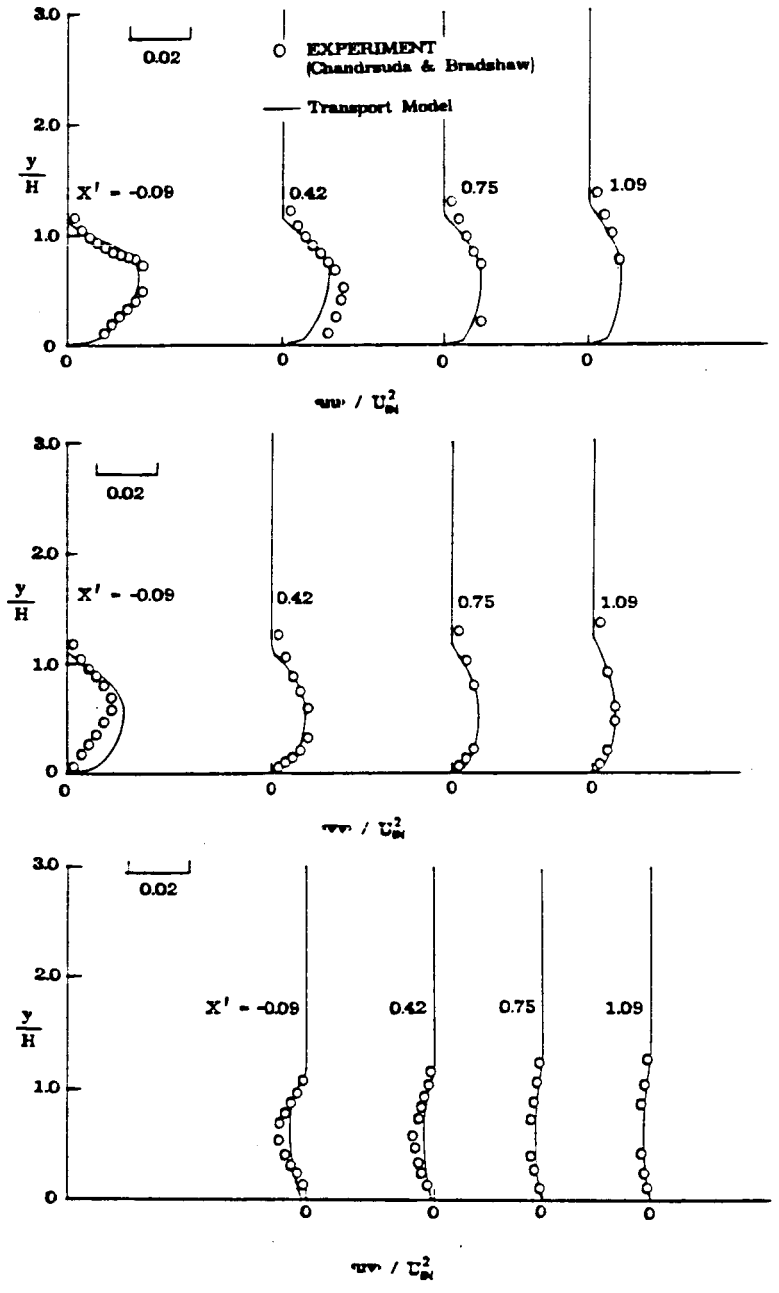

FIGURE 6. Reynolds-stress profiles downstream of the step.

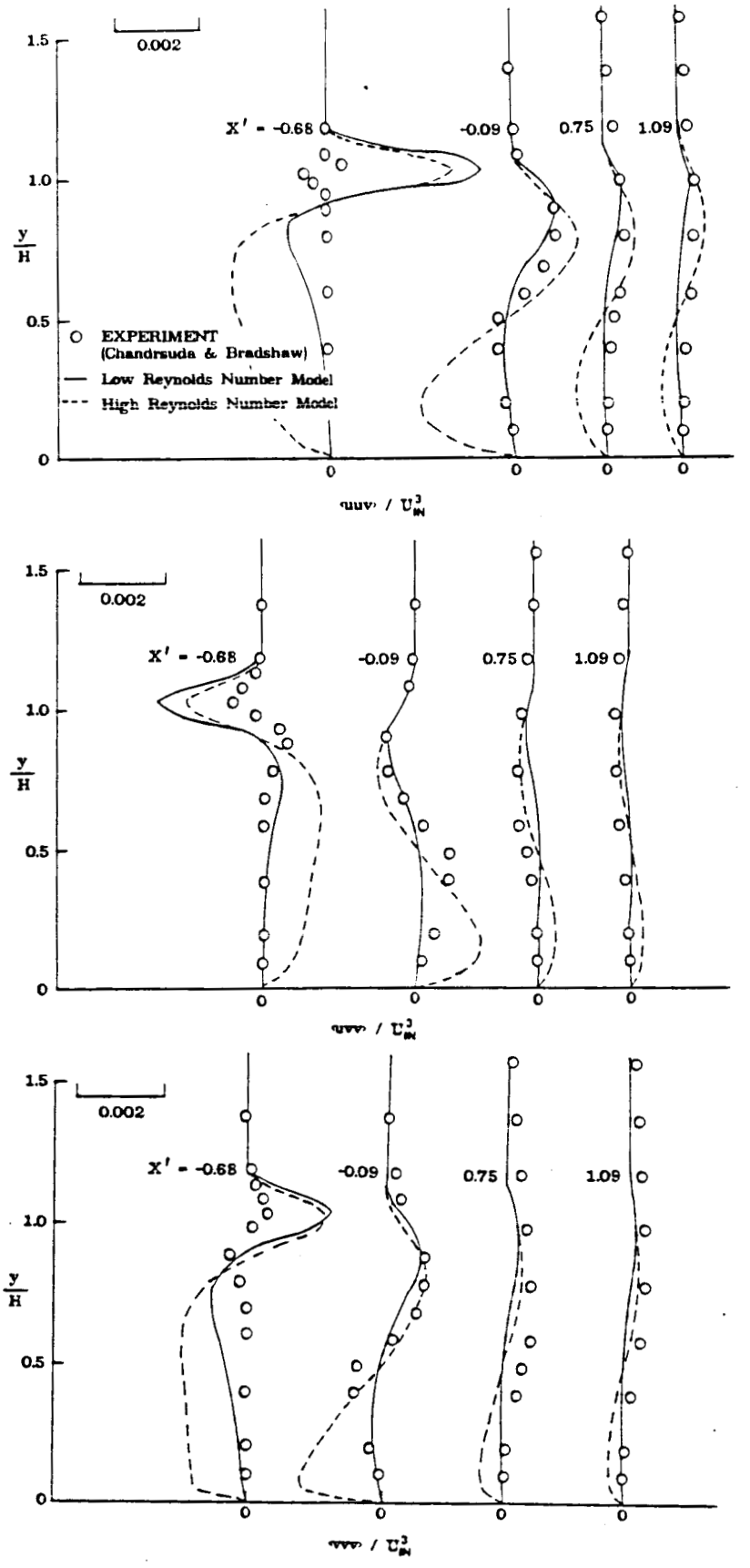

FIGURE 7. Third-moment profiles downstream of the step: Comparison of the low and high-Reynolds number models.

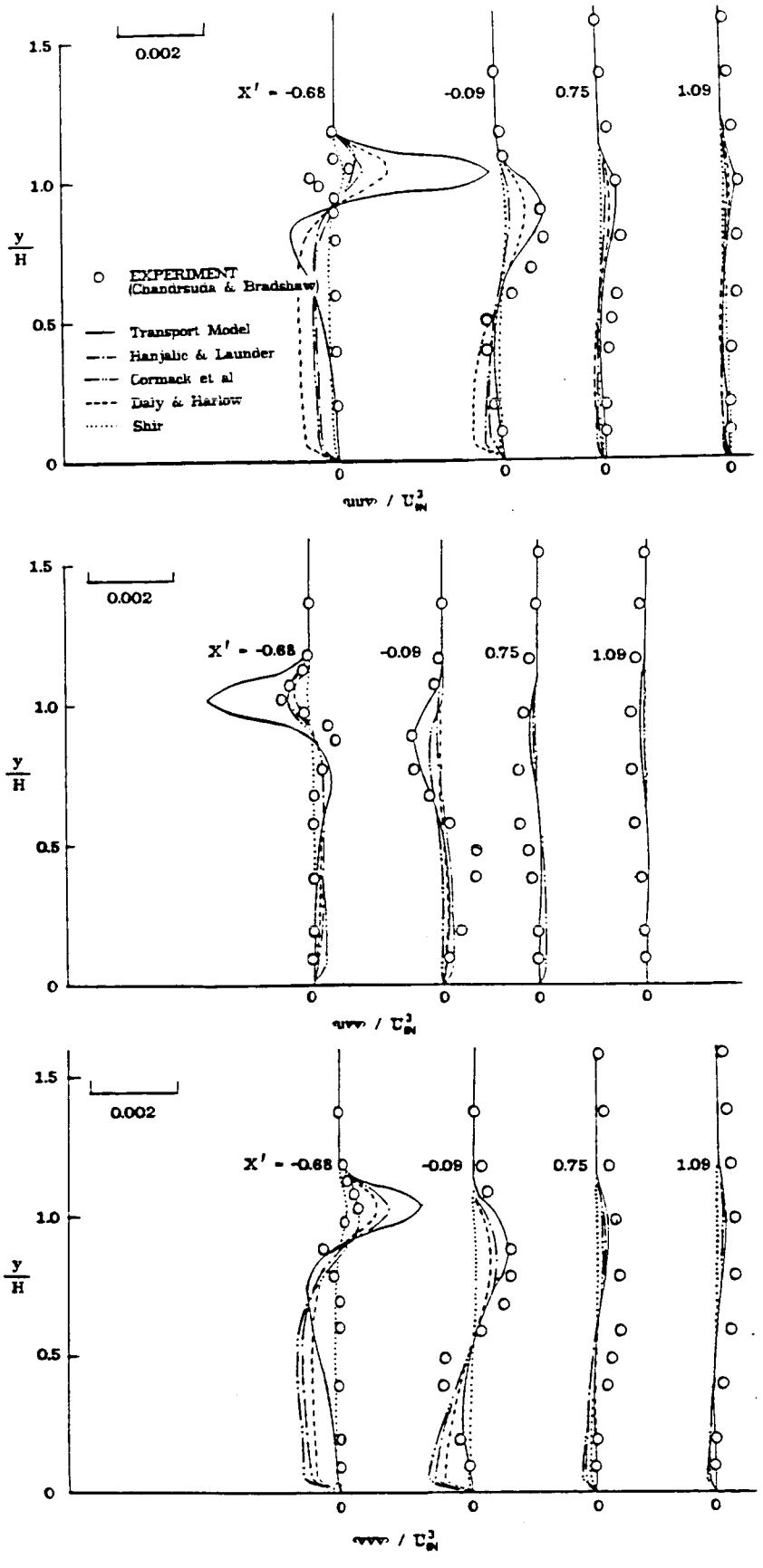

FIGURE 8. Third-moment profiles downstream of the step: Comparison of the low-Reynolds number model with algebraic models.

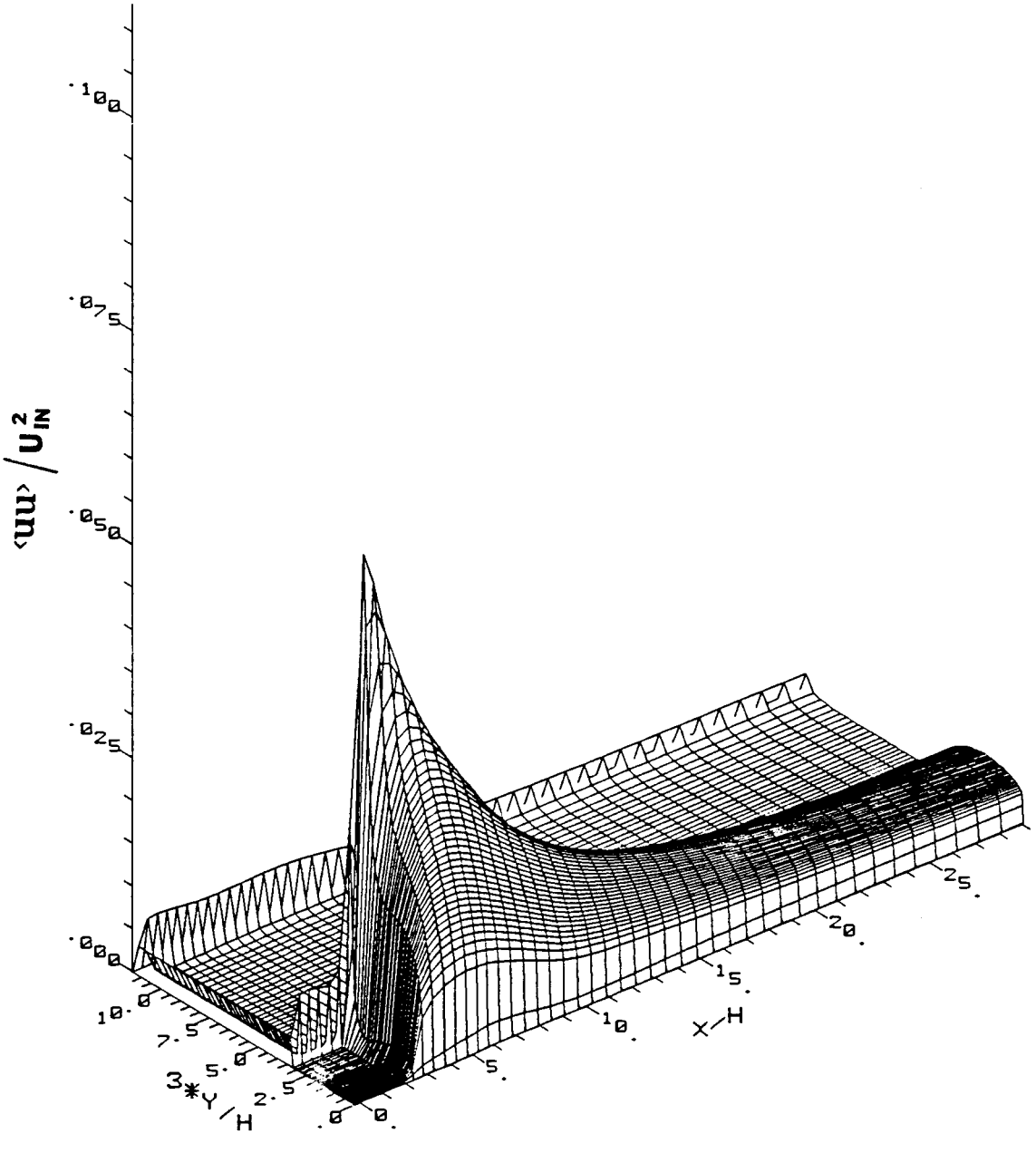

FIGURE 9. Variation of $\langle u^2 \rangle$

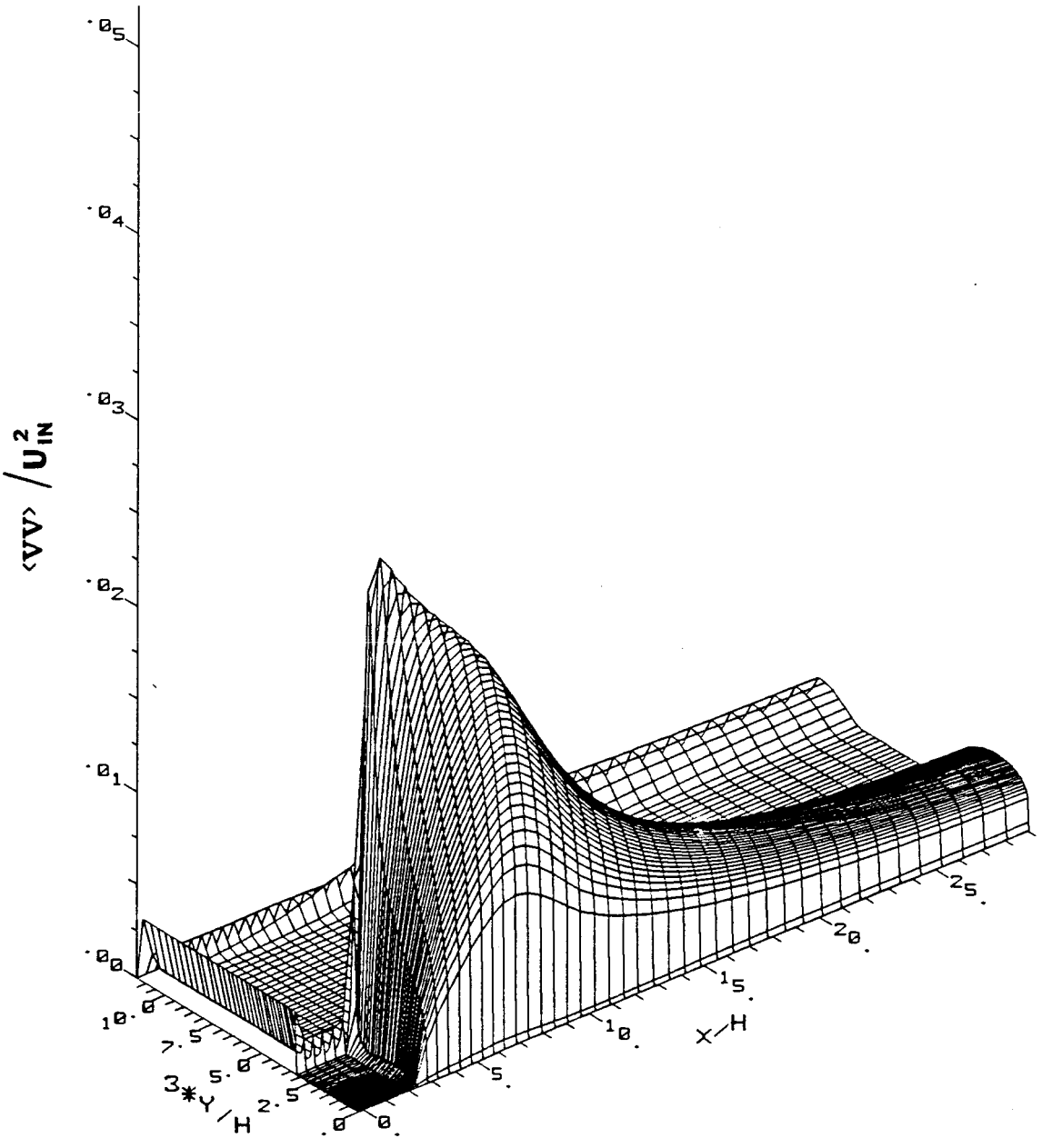

FIGURE 10. Variation of $\langle v^2 \rangle$

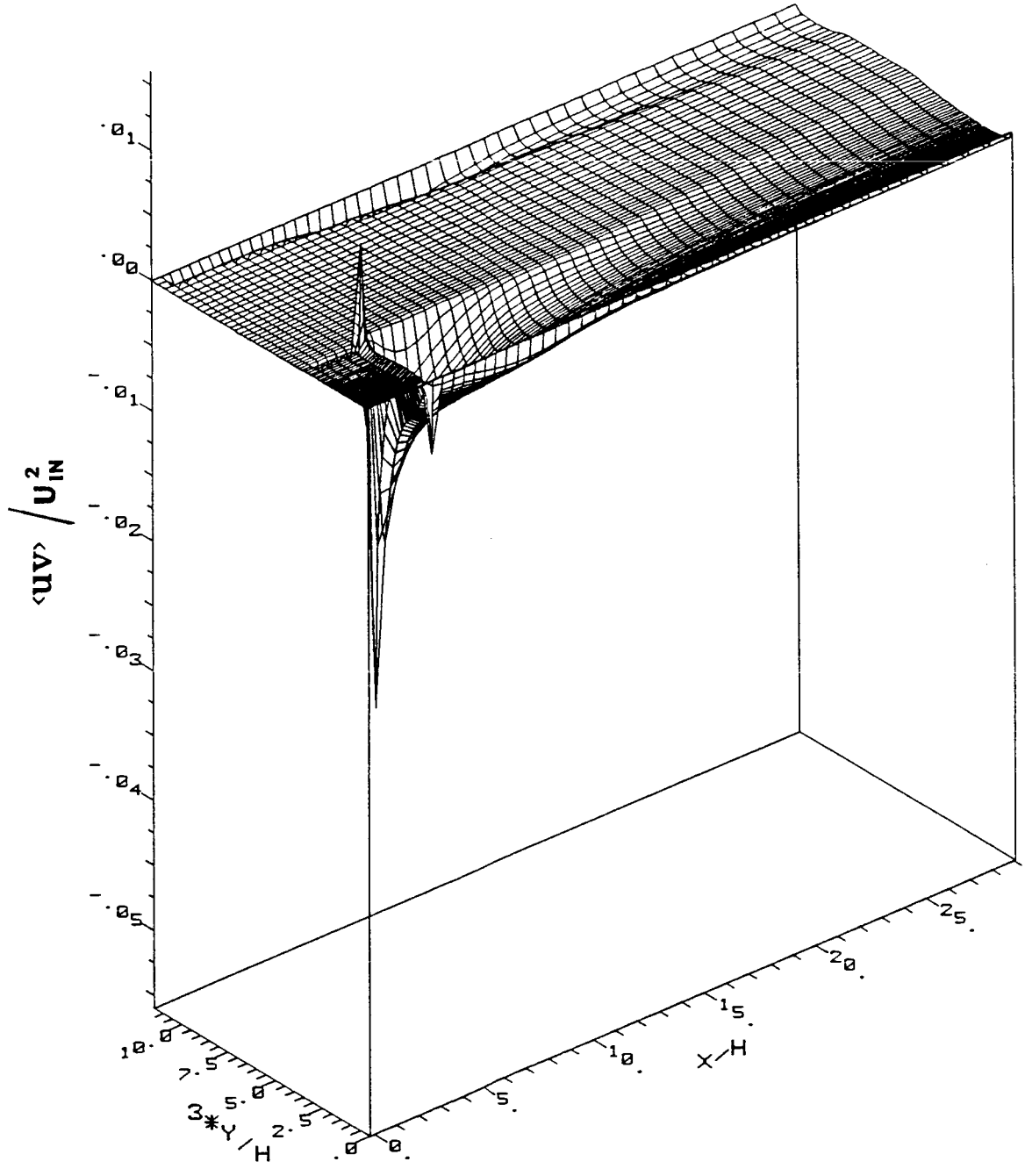

FIGURE 11. Variation of <uv>

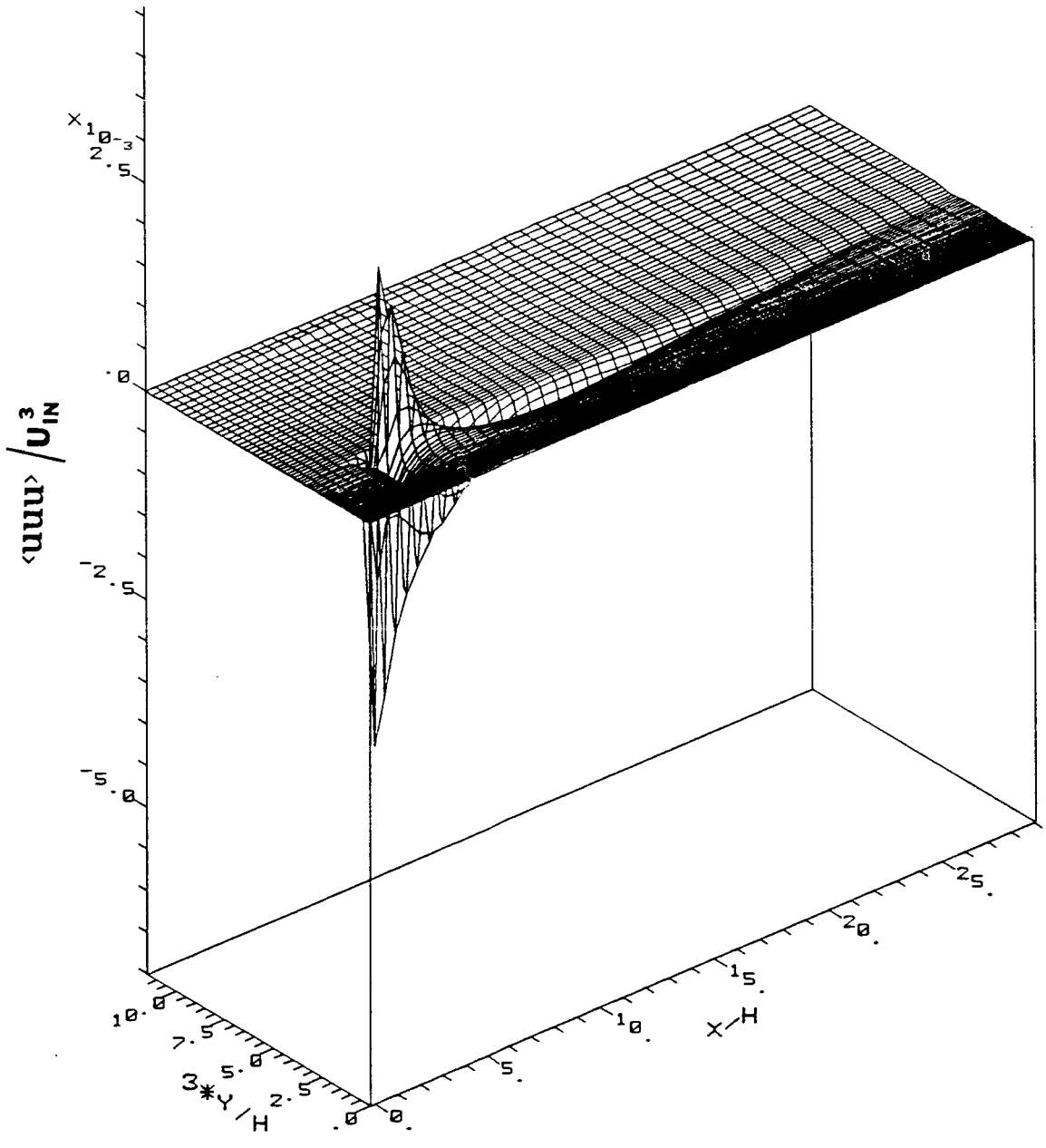

FIGURE 12. Variation of $\langle u^3 \rangle$

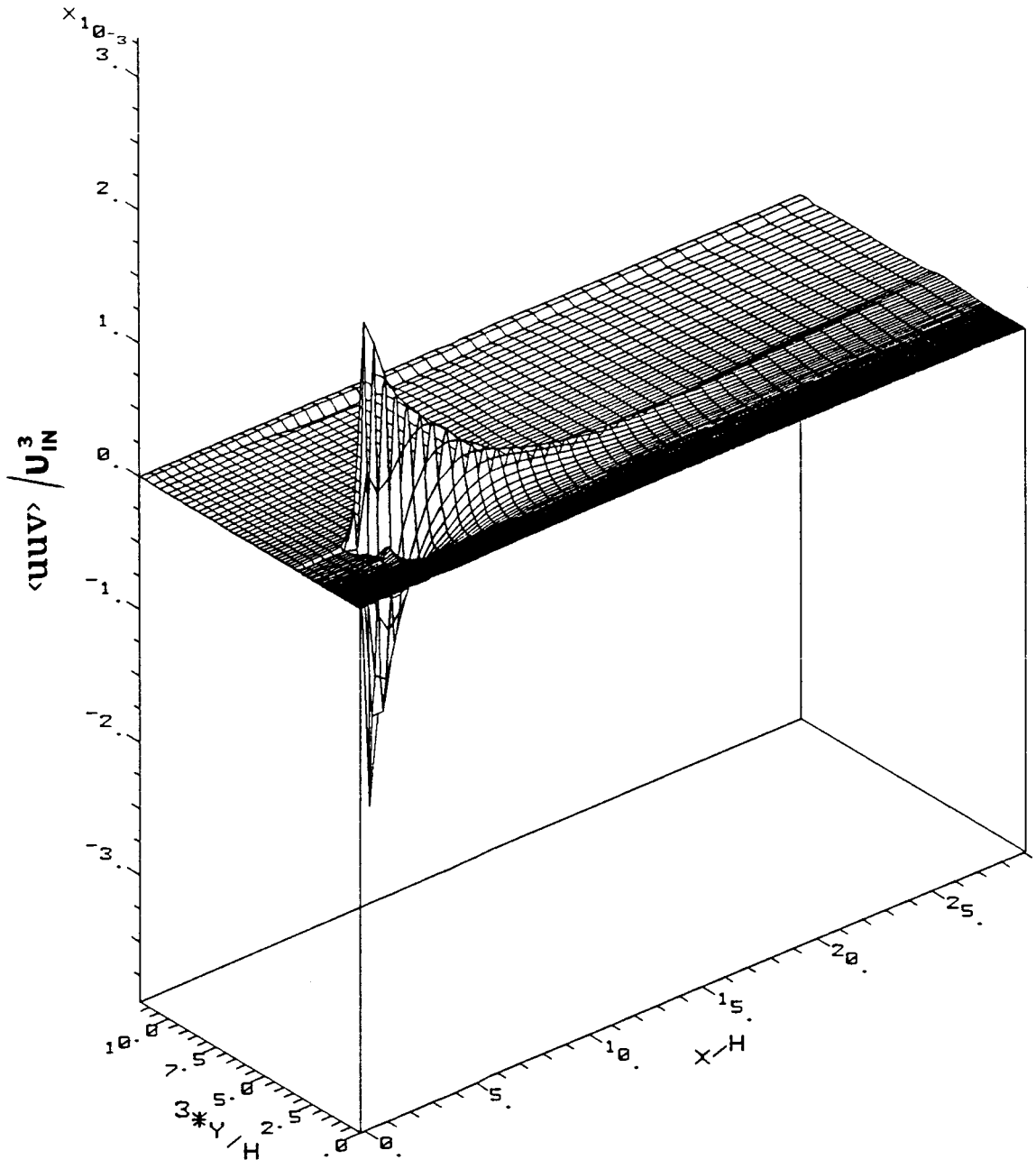

FIGURE 13. Variation of $\langle u^2v \rangle$

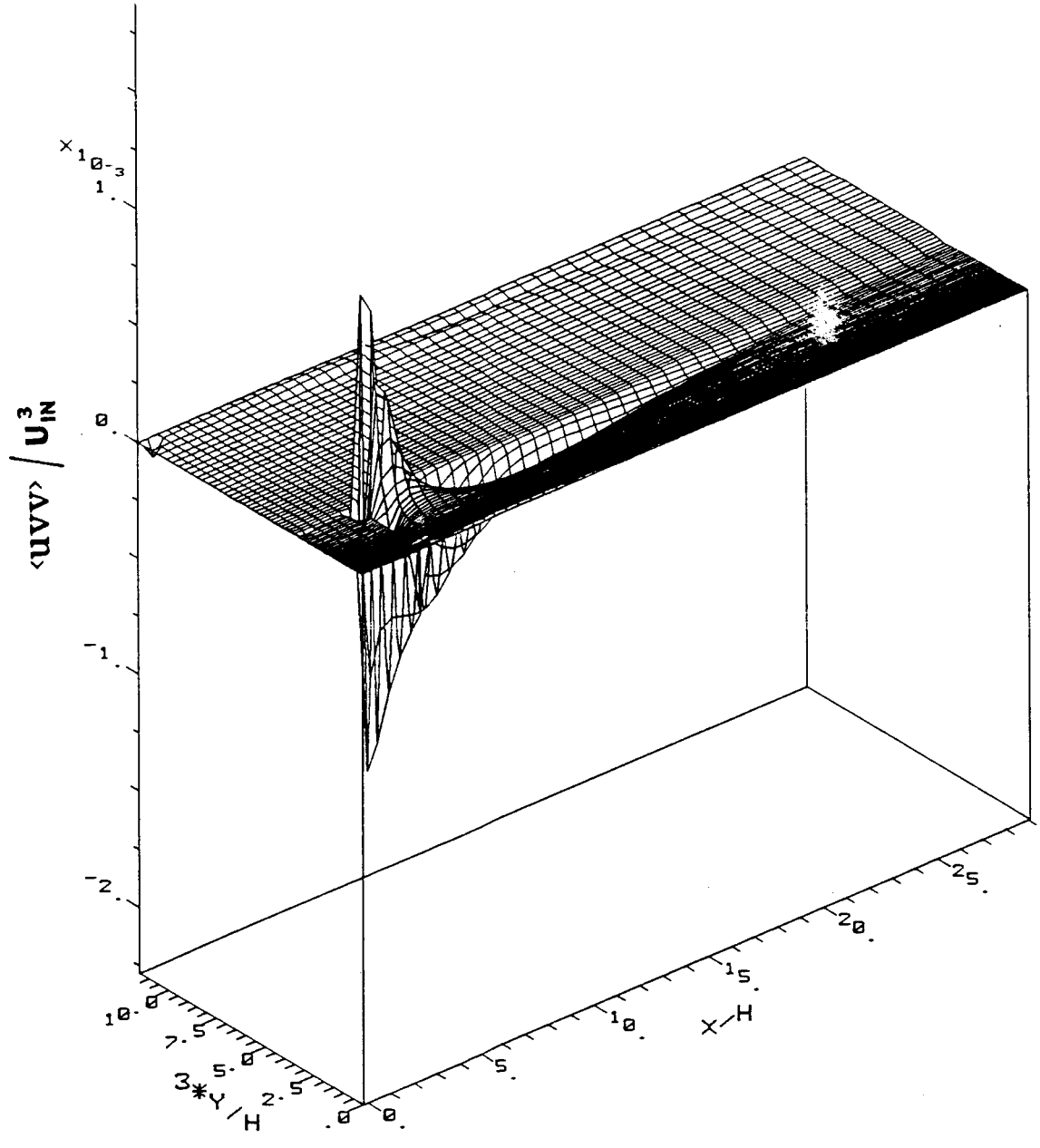

FIGURE 14. Variation of $\langle uv^2 \rangle$

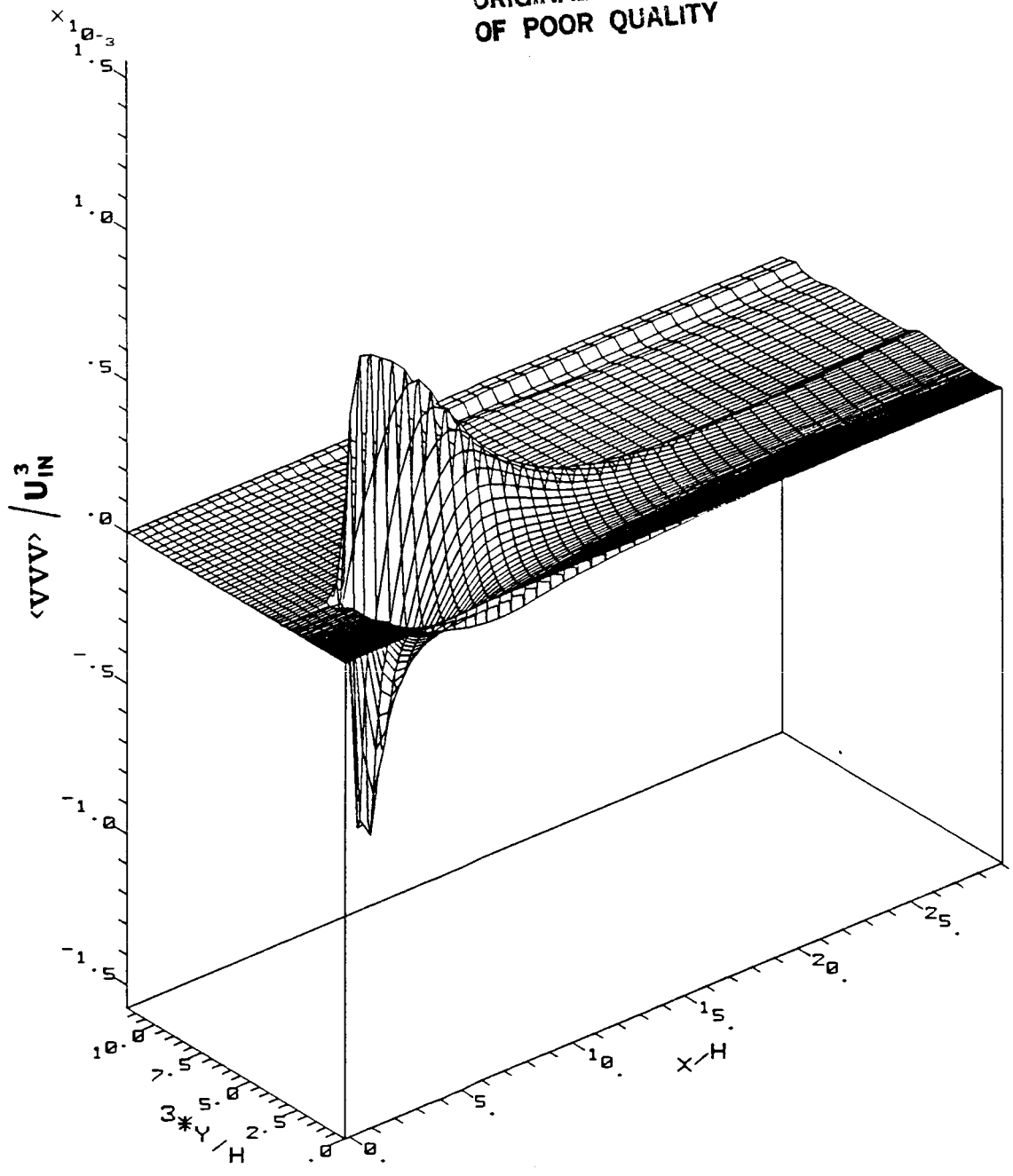

FIGURE 15. Variation of $\langle v^3 \rangle$